Local study of Lithium Niobate domain walls

Presenter name and spokesperson

Dr. Juliana Heiniger-Schell

Second spokesperson

Prof. Lukas Eng

Collaboration CERN-INTC-2024-034 / INTC-P-703

J. H.-Schell[1,2], H. M. Gürlich[3], T. T. Dang[2], I. C. J. Yap[2], B. Dörschel[2], S. D. Seddon[3], B. Koppitz[3], A. M. L. Lopes[4], A. W. Carbonari[5], N. Lima[1,5], P. Rocha-Rodrigues[4], L. M. Eng[3,6]

[1] European Organization for Nuclear Research (CERN), CH-1211 Geneva, Switzerland

[2] Institute for Materials Science and Center for Nanointegration Duisburg-Essen (CENIDE), University of Duisburg-Essen, 45141 Essen, Germany

[3] Institute of Applied Physics, Technische Universität Dresden, 01062 Dresden, Germany

[4] Institute of Physics for Advanced Materials, Nanotechnology and Photonics (IFIMUP), 4169 - 007 Porto, Portugal

[5] Instituto de Pesquisas Energéticas e Nucleares IPEN-CNEN/SP, São Paulo 05508-000, Brazil

[6] ct.qmat: Dresden-Würzburg Cluster of Excellence—EXC 2147, Technische Universität Dresden, 01062 Dresden, Germany

Lithium Niobate

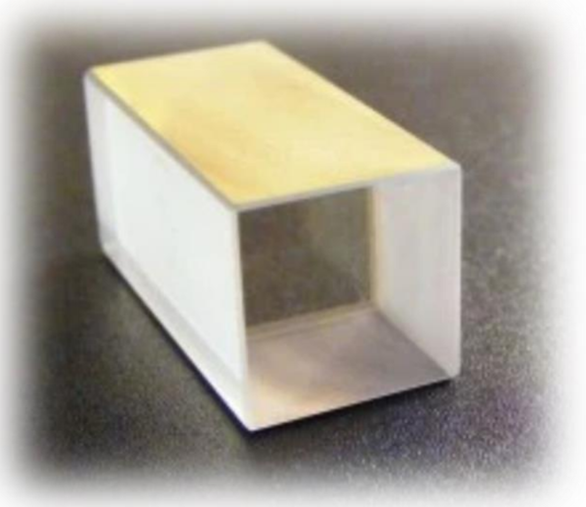

- **Robust wide-band-gap ferroelectric** ($E_g \approx 4$ eV)
- **High Curie temperature** ($T_c \approx 1200$ °C)
- **Large values of the spontaneous polarization near room temperature (**$P_S \approx 70$ μC/cm^2)
- **The 5-%Mg doping level leads to a two-order higher optical stability**

References:

C. S. Werner et al., Sci Rep 7, 9862 (2017). https://doi.org/10.1038/s41598-017-09703-2

Y. Furukawa et al., Jpn. J. Appl. Phys. 35 (1996) 2740. https://dx.doi.org/10.1143/JJAP.35.2740

Domain Walls (DW)

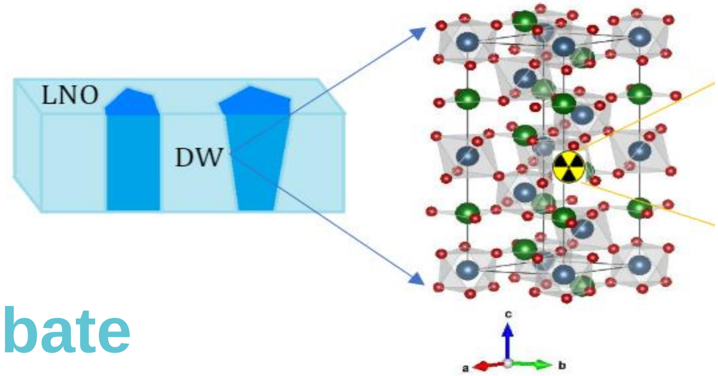

General

- Ferroelectric domain walls isolate regions with different polarizations.
- Due to the local breaking of spatial symmetry, DW can exhibit properties completely different from those of the material

Lithium Niobate

- Charged ferroelectric domain walls (CDW) in LNO have a 13-order higher conductivity than in bulk.
- New applications: adaptive-optical elements, electrically controlled integrated-optical chips for quantum photonics, and advanced LN-semiconductor-hybrid optoelectronic devices

References:

C. S. Werner et al., Sci Rep 7, 9862 (2017). https://doi.org/10.1038/s41598-017-09703-2

R. K. Vasudevan, et al. Adv. Funct. Mater. 23 (2013) 2592. https://doi.org/10.1002/adfm.201300085

C. S. Werner et al., Scientific Reports 7 (2017) 9862. https://doi.org/10.1038/s41598-017-09703-2

Applications current state of art and future

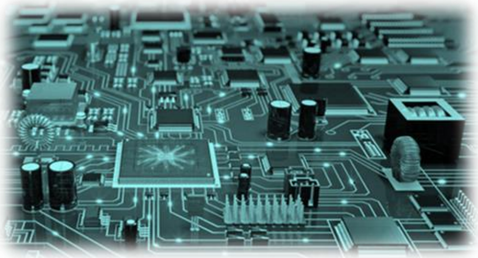

LNO in nanoelectronics

- Sensors in compact eletromechanical systems
- Selectors in phase-change memory and resistive random access memory
- Half-wave/full wave rectifiers in modern nanocircuits.

The role of DW in performance

- Conduction through head-to-head, neutral or tail-to-tail DWs
- High conductivity between polarization orientations
- Ultra-thin topological interface (~few units cells)
- “DW electronics’

References:

J. Sun et al., ACS Appl. Mater. Interfaces 2023, 15, 6, 8691–8698 (https://pubs.acs.org/doi/full/10.1021/acsami.2c20579)

D. Hu et al., IEEE 2024 (https://ieeexplore.ieee.org/abstract/document/10373934)

H. Beccard et al., Phys. Rev. Appl. 2023 (https://journals.aps.org/prapplied/abstract/10.1103/PhysRevApplied.20.064043)

.

Applications current state of art and future

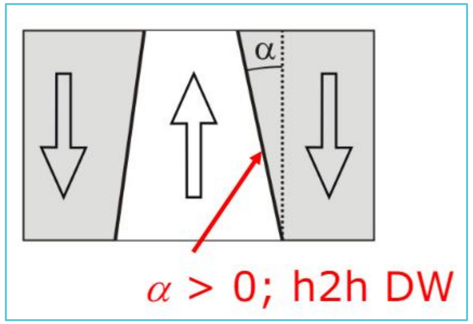

The role of DW in performance

- Inclined DWs (a > 0) in LNO lead to DW conductivity (DWC) of up to 1 mA [Kirbus2019, Godau2017]
- h2h vs. t2t, i.e. n-type / p-type DWs in PPLN are re-configurable [Xiao2018]
- DWC transport activation energies (20 … 400 °C of ~ 120 meV [Kämpfe2020, Yakhnevych2024]
- Bloch-, Néel-type DW topology in LNO [Acevedo-Salas2023]
- Hall-transport of inclined h2h DWs in LNO show 2D-electron-gas behavior [Beccard2024, Verhoff2024, Yakhnevych2024]
- Separating Schottky barrier injection from true electronic DW transport through the R2D2-model [Zahn2024]
- Enhanced DWC by photo-generated electron-hole pairs [Ding2024]
- Mechanical strain in-/decreases DWC depending on DW orientation [Singh2021]

Works of the group Prof. Lukas Eng (TU-Dresden)

- L. M. Verhoff, L.M. Eng, et al., 2-dimensional electronic conductivity in insulating ferroelectrics: Peculiar properties of domain walls, Phys. Rev. Lett. (2024) submitted.
- U. Yakhnevych, L.M. Eng, et al., High-temperature domain wall current in Mg-doped lithium niobate single crystals up to 400°C, Appl. Phys. Lett. (2004) submitted; https://doi.org/10.48550/arXiv.2404.01214.
- L. Ding, L.M. Eng, et al., Comparative study of photo-induced electronic transport along ferroelectric domain walls in lithium niobate single crystals, Appl. Phys. Lett. (2024) submitted; https://arxiv.org/abs/2402.17508.
- M. Zahn, L.M. Eng, et al., Equivalent-circuit model that quantitatively describes domain-wall conductivity in FE $LiNbO_3$, Phys. Rev. Appl. 21, 024007 (2024); https://doi.org/10.1103/PhysRevApplied.21.024007.
- H. Beccard, L.M. Eng, et al., Hall mobilities and sheet carrier densities in a single $LiNbO_3$ conductive ferroelectric DWs, Phys. Rev. Appl. 20, 064043 (2023); https://doi.org/10.1103/PhysRevApplied.20.064043.
- U. Acevedo-Salas, L.M. Eng, et al., Impact of 3D curvature on the polarization orientation in nonIsing domain walls, Nano Letters 23, 795 (2023); https://doi.org/10.1021/acs.nanolett.2c03579.
- E. Singh, L.M. Eng, et al., Tuning the domain wall conductivity in bulk lithium niobate by uniaxial stress, Phys. Rev. B 106, 144103 (2022); https://doi.org/10.1103/PhysRevB.106.144103

Works of the group Prof. Lukas Eng (TU-Dresden)

- J. Rix, L.M. Eng, et al., Brillouin and Raman imaging of domain walls in periodically-poled MgO:$LiNbO_3$, Optics Express 30, 5051 (2022); https://doi.org/10.1364/OE.447554.
- J. Golde, L.M. Eng, et al., Quantifying the Refractive Index of Ferroelectric Domain Walls in Periodically-Poled $LiNbO_3$ Single Crystals by Polarization-Sensitive Optical Coherence Tomography, Optics Expr. 29, 33615 (2021); https://doi.org/10.1364/OE.432810.
- Th. Kämpfe, L.M. Eng, et al., Tunable Non-Volatile Memory by Conductive FE Domain Walls in Lithium Niobate Thin Films, Crystal 10, 804 (2020); https://doi.org/10.3390/cryst10090804.
- B. Kirbus, L.M. Eng, et al., Real-Time 3D-Imaging of Nanoscale Ferroelectric Domain Wall Dynamics in Lithium Niobate Single Crystals under Electric Stimuli: Implications for Domain Wall-Based Nanoelectronic Devices, ACS Applied Nano Materials 2, 5787 (2019); https://doi.org/10.1021/acsanm.9b01240.
- S.Y. Xiao, L.M. Eng, et al., Dipole-tunneling model from asymmetric DW conductivity in $LiNbO_3$ single crystals, Phys. Rev. Appl. 10, 034002 (2018); https://doi.org/10.1103/PhysRevApplied.10.034002.
- Ch. Godau, L.M. Eng, et al., Enhancing the domain wall conductivity in lithium niobate single crystals, ACS Nano 11, 4816 (2017); https://doi.org/10.1021/acsnano.7b01199.
- T. Kämpfe, L.M. Eng, et al., Optical 3D profiling of charged DWs in ferroelectrics by Cherenkov SHG, Phys. Rev. B 89, 035314 (2014); https://doi.org/10.1103/PhysRevB.89.035314.

Perturbed Angular Correlation (PAC)

A method to probe hyperfine interactions in matter

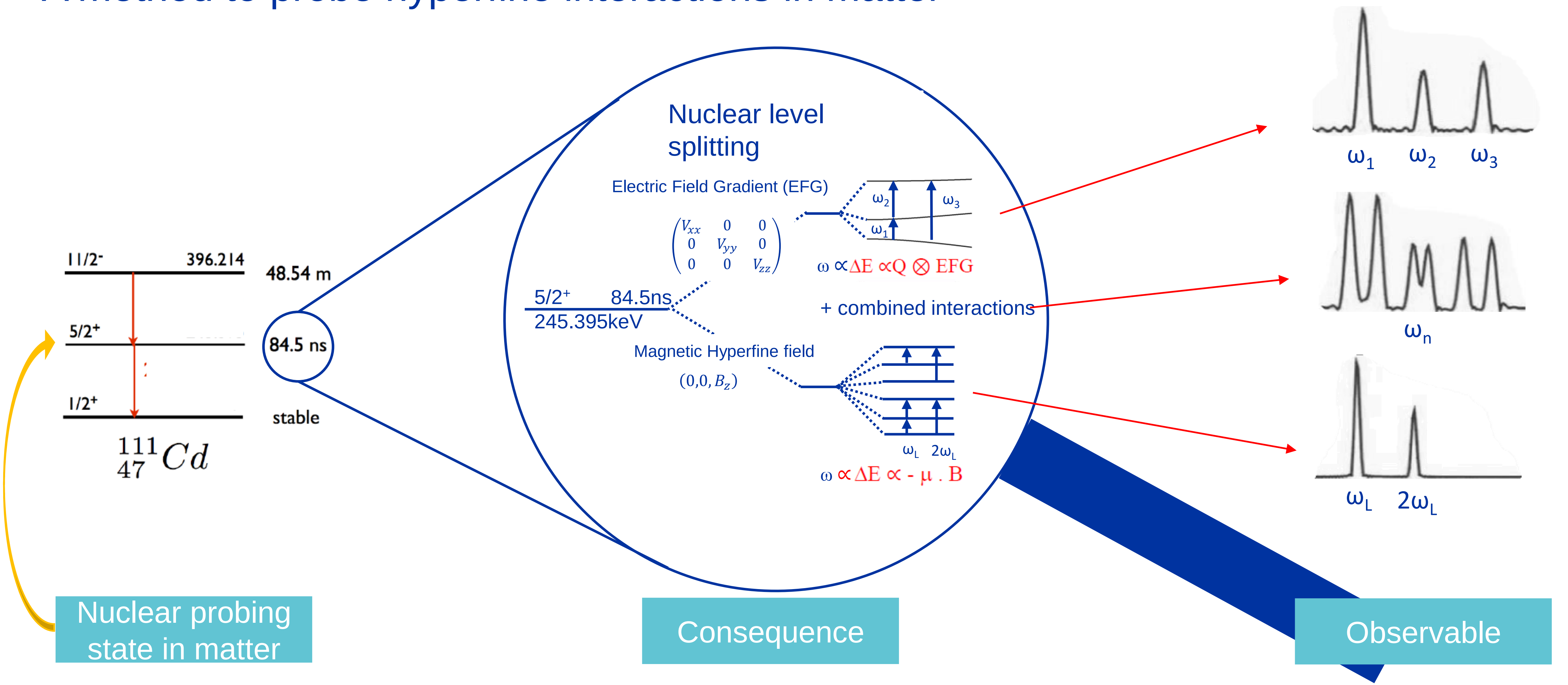

Nuclear level splitting

Electric Field Gradient (EFG)

$$\begin{pmatrix} V_{xx} & 0 & 0 \\ 0 & V_{yy} & 0 \\ 0 & 0 & V_{zz} \end{pmatrix}$$

$\omega \propto \Delta E \propto Q \otimes EFG$

+ combined interactions

Magnetic Hyperfine field

$(0,0,B_z)$

$\omega \propto \Delta E \propto -\mu \cdot B$

Transition frequencies

Nuclear probing state in matter

Consequence

Observable

The frequencies

Quadrupole frequency: $\omega_Q = \frac{eQV_{zz}}{4I(2I-1)\hbar}$

Spin independent: $\nu_Q = \frac{eQV_{zz}}{h}$

Lowest observable transition frequency
for half-integer spin and $\eta = 0$:

$$\omega_0 = 6\omega_Q$$

$$\omega_n = n\omega_0 \ (n = 1,2,3 \text{ for } I = 5/2)$$

For $\eta \neq 0$ and $I = 5/2$

$$\omega_1 = 2\sqrt{3}\alpha\omega_q \sin\left(\frac{1}{3}\arccos(\beta)\right),$$

$$\omega_2 = 2\sqrt{3}\alpha\omega_q \sin\left(\frac{1}{3}[\pi - \arccos(\beta)]\right),$$

$$\omega_3 = 2\sqrt{3}\alpha\omega_q \sin\left(\frac{1}{3}[\pi + \arccos(\beta)]\right),$$

$$\alpha = \sqrt{\frac{28(3+\eta^2)}{3}},$$

$$\beta = \frac{80(1-\eta^2)}{\alpha^3}.$$

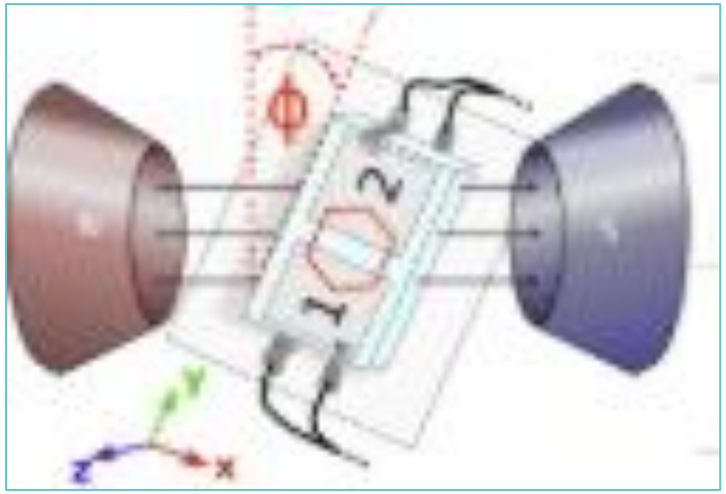

The EFG in LNO

LNO properties ⟷ Nuclear probe properties ✚ Nuclear probe incorporation method and measurements conditions

Apply fields

Vzz and η values

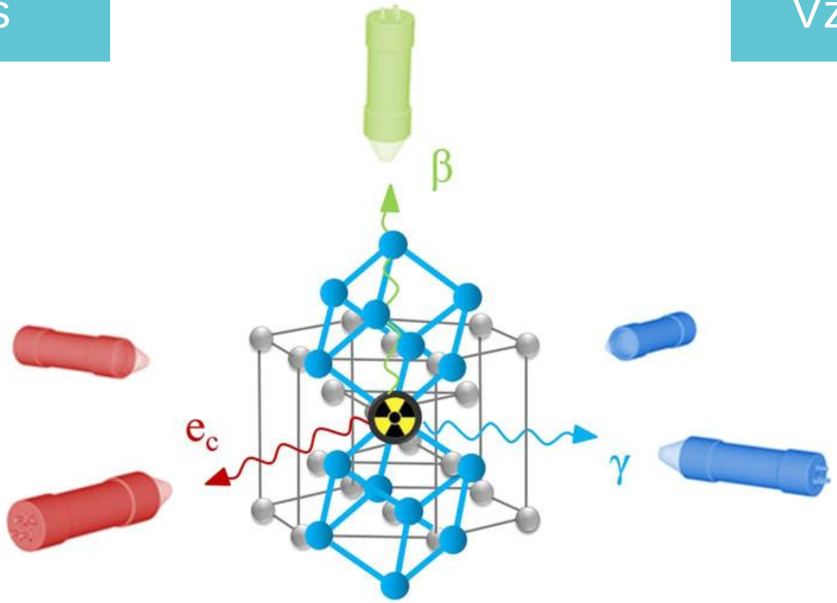

Conduction electrons (DWs)

Electrons bound to the probe

AIP Advances 7, 105017 (2017)
https://doi.org/10.1063/1.4994249

Defects and lattice deformation

Lattice location of the probe

Previous TDPAC measurements

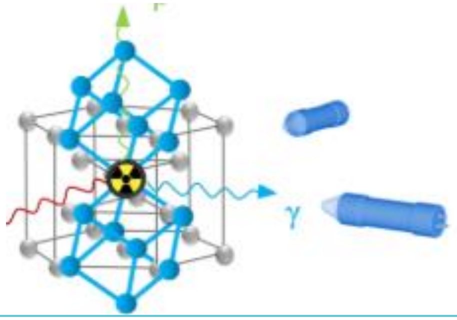

^{111m}Cd implanted in LNO at 60 keV (ISOLDE)

Figure source: B. Hauer et al. Phys. Rev. B 51, 6208 (1995).

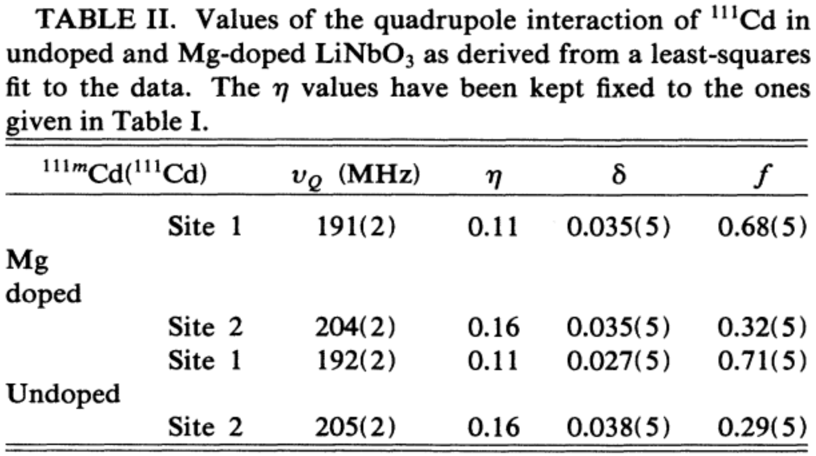

TABLE II. Values of the quadrupole interaction of ^{111}Cd in undoped and Mg-doped LiNbO$_3$ as derived from a least-squares fit to the data. The η values have been kept fixed to the ones given in Table I.

^{111m}Cd(^{111}Cd)		ν_Q (MHz)	η	δ	f
Mg doped	Site 1	191(2)	0.11	0.035(5)	0.68(5)
	Site 2	204(2)	0.16	0.035(5)	0.32(5)
Undoped	Site 1	192(2)	0.11	0.027(5)	0.71(5)
	Site 2	205(2)	0.16	0.038(5)	0.29(5)

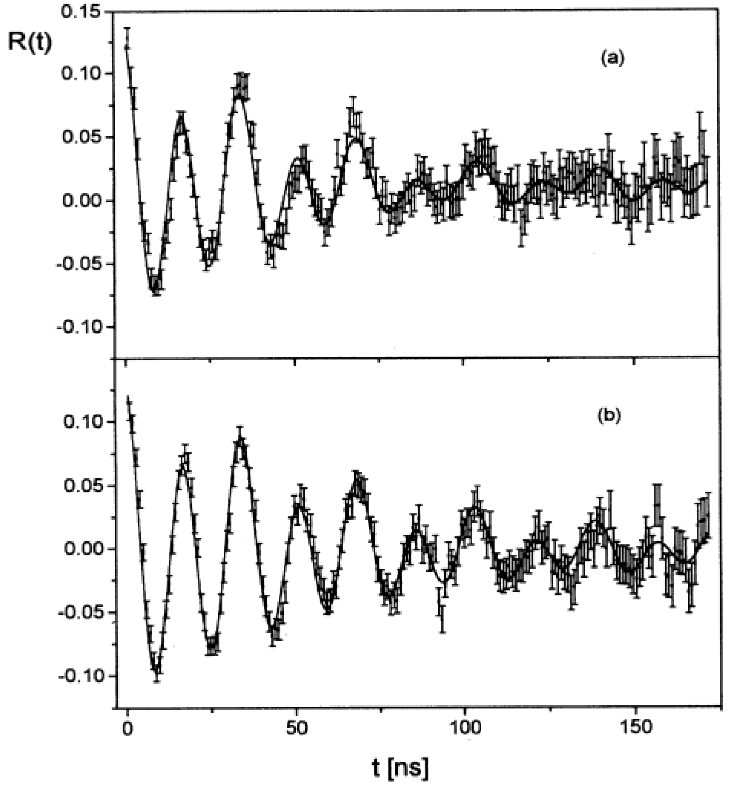

FIG. 6. Time-dependent anisotropy of the 151–245 keV γ-γ cascade of ^{111}Cd(^{111}Cd) after annealing for 30 min at 970 K in Mg-doped (a) and undoped LiNbO$_3$ (b).

Previous TDPAC measurements

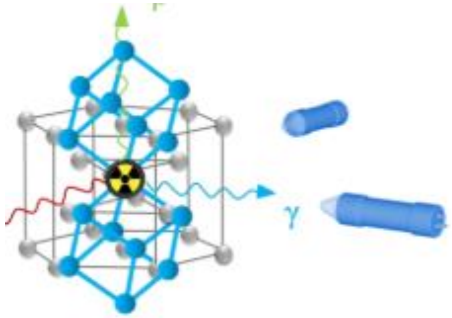

^{111}In implanted in LNO at 150 keV

Figure source: B. Hauer et al. Phys. Rev. B 51, 6208 (1995).

v_{Q1} = 192(1) MHz and asymmetry parameter η = 0.11(2) (predominant 68%) and v_{Q1} = 205(1) MHz and η = 0.16(4).

Second fraction for In@Li associated to a Nb-vacancy.

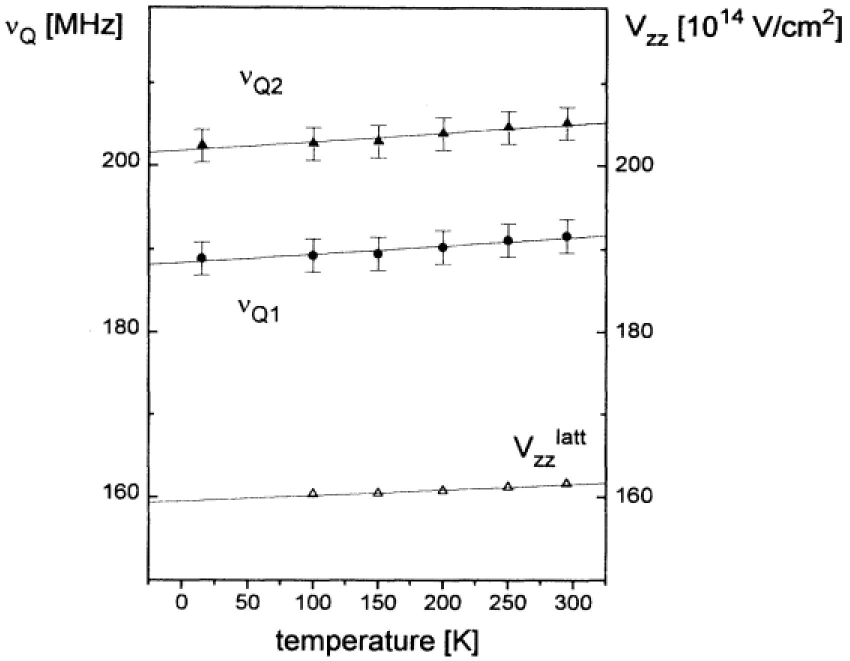

FIG. 5. Variation of v_{Q1} and v_{Q2} with the sample temperature. For comparison the EFG value V_{zz}^{latt} calculated in the point charge model (see text) for the corresponding lattice parameters is shown in the lower part.

Previous TDPAC measurements

Obtained NQI for ^{111m}Cd 60 keV at ISOLDE

Figure source: A. Kling, et al., Nucl. Instr. Meth. B 1996, 113, 293–295. https://doi.org/10.1016/0168-583X(95)01329-6

ν_Q = 191(2) MHz and asymmetry parameter η = 0. The asymmetry parameter indicate a higher crystal lattice.

Other references: LN (4.6 wt% K2O)

A. Kling, J.G. Marques, Crystals 2021, 11, 501.

https://doi.org/10.3390/cryst1105050

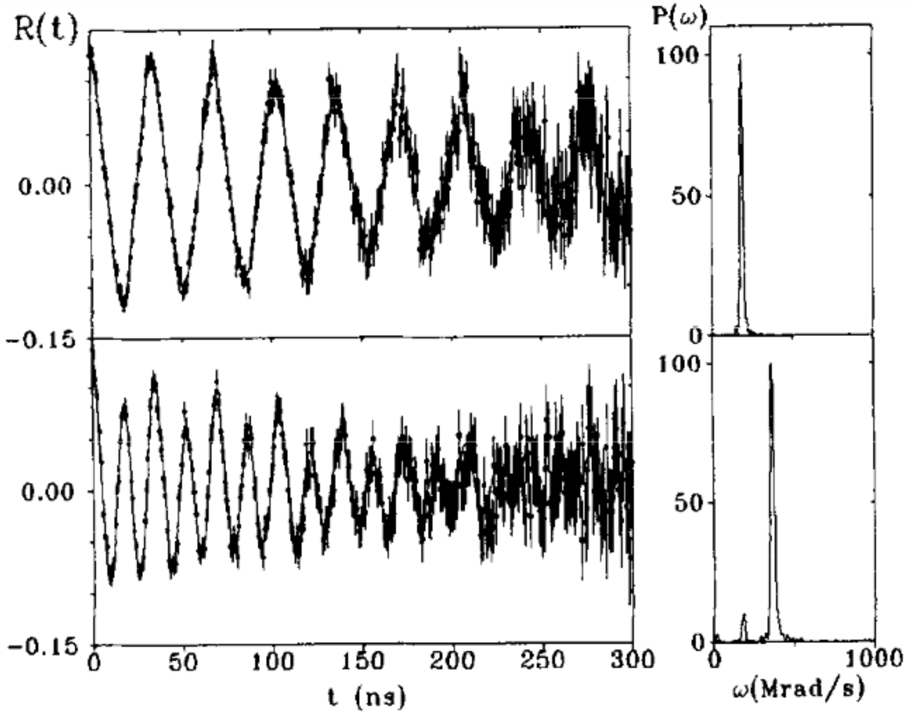

Fig. 4. Time dependent anisotropy of the 151–245 keV e^-–γ cascade of ^{111}Cd in near-stoichiometric $LiNbO_3$, with c-axis perpendicular to the detectors' plane (top), and c-axis in the detectors' plane at 45° with two detectors (bottom).

Previous TDPAC measurements

Obtained NQI for ^{111}In 150 keV at HISKP

Figure source: J.G. Marques, et al., Rad. Eff. Def. Solids 1999, 150, 233–236. https://doi.org/10.1080/10420159908226235

ν_{Q1} = 191(2) MHz and ν_{Q2} = 205.2 MHz and asymmetry parameter $\eta > 0$. Two distinct Li-sites. Lattice disorder decreases with increase of K_2O (lower delta value).

Data could not be described by models that consider vacancies and Nb antisites.

Other references: LN (4.6 wt% K2O)

A. Kling, J.G. Marques, Crystals 2021, 11, 501.

https://doi.org/10.3390/cryst1105050

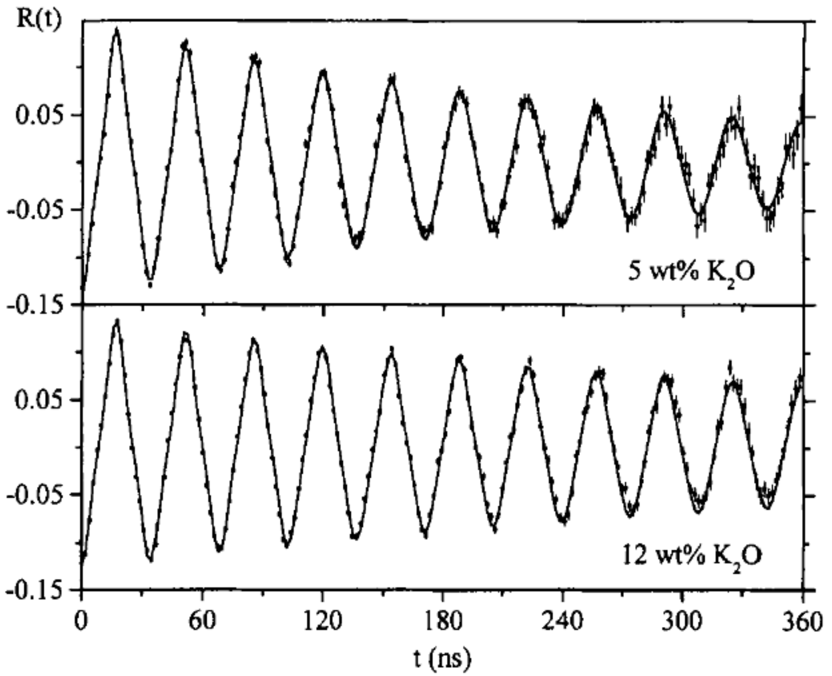

FIGURE 1 PAC spectra obtained in the K5 and K12 crystals.

Our TDPAC measurements

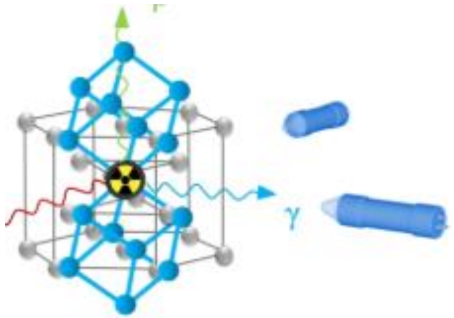

Spectra

R(t) Single Domain Periodically poled

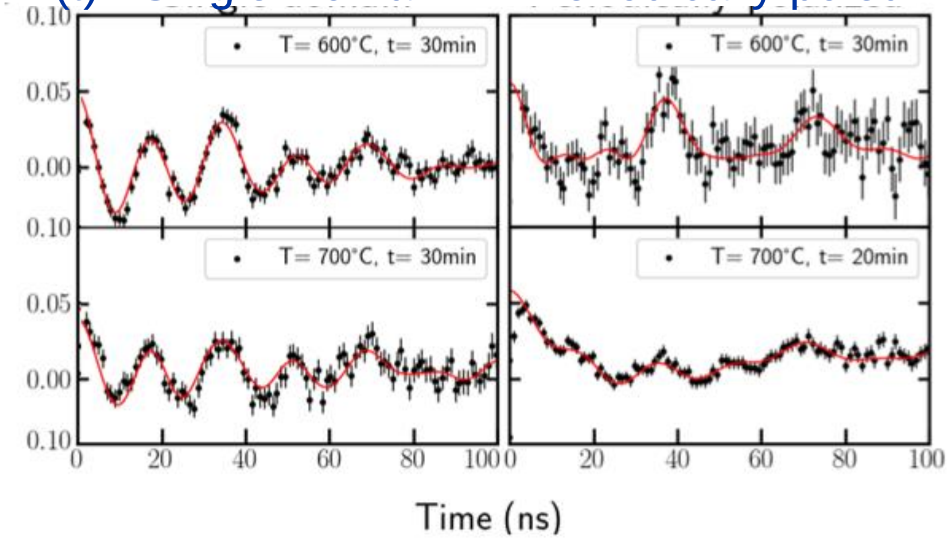

Comparison with DFT and previous work

System	Charge of System	$V_{33}^{DFT}(V/A^2)$	η^{DFT}	$\Delta H^{DFT}(eV)$	$\omega_0^{DFT}[Mrad/s]$
Cd_{Li}	+1	90.956	0.000	-1.9529	172(1)
Cd_{Li}	0	89.243	0.000	4.8395	168(1)
Cd_{Li} with Li vacancy	0	91.726	0.106	8.5434	173(1)
		$V_{33}^{Exp}(V/A^2)$	η^{Exp}		$\omega_0^{Exp}[Mrad/s]$
Present study (*Single domain, T = 600 °C*)	-	95.3(4)	0	-	180.4(7)
Present study (*Single domain, T = 700 °C*)	-	96.2(1)	0	-	182(1)
[20] site 1	-	93.9(1)	0.11(2)	-	180(1)
[20] site 2	-	98.8(2)	0.16(4)	-	192(1)

Table 1: Relevant parameters for the Cd(LNO) calculation (^{DFT}) and experimental values (^{Exp}). Note that the reported values in $\Delta H^{DFT}(eV)$ are taken with reference to the equivalent LNO supercell system without any defects.

Beam request ^{111m}Cd 9 shifts (72 hours) + 1 shift reserved

Probe	Annealing	Number of samples (5 angular dependence measurements + reproduction)	Beam time
Single domain 30 keV (repeat for 60 keV)	air	10 +10	10 hours
	Oxygen flow	10 +10	10 hours
	Ar flow	10 +10	10 hours
Periodically poled 30 keV (repeat for 60 keV)	air	10 +10	10 hours
	Oxygen flow	10 +10	10 hours
	Ar flow	10 +10	10 hours
Single domain 30 keV applied E field (repeat for 60 keV)	air	2 +2	2 hours
	Oxygen flow	2 +2	2 hours
	Ar flow	2 +2	2 hours
Periodically poled 30 keV applied E field (repeat for 60 keV)	air	2 +2	2 hours
	Oxygen flow	2 +2	2 hours
	Ar flow	2 +2	2 hours

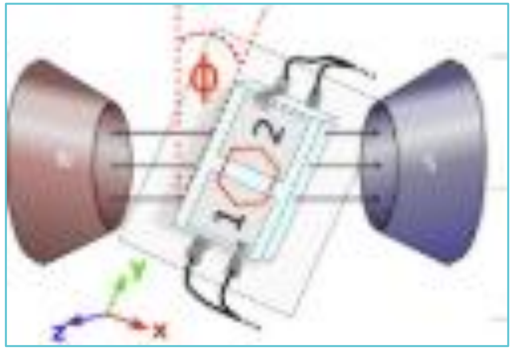

Beam request ^{111}In 2 shifts

Probe	Annealing	Number of samples (~10 angular dependence measurements + reproduction)	Beam time
Single domain 30 keV (repeat for 60 keV)	air	1 +1	2 hours
	Oxygen flow	1 +1	2 hours
	Ar flow	1 +1	2 hours
Periodically poled 30 keV (repeat for 60 keV)	air	1 +1	2 hours
	Oxygen flow	1 +1	2 hours
	Ar flow	1 +1	2 hours
Single domain 30 keV applied E field (repeat for 60 keV)	air	1 +1	2 hours
	Oxygen flow		
	Ar flow		
Periodically poled 30 keV applied E field (repeat for 60 keV)	air	1 +1	2 hours
	Oxygen flow		
	Ar flow		

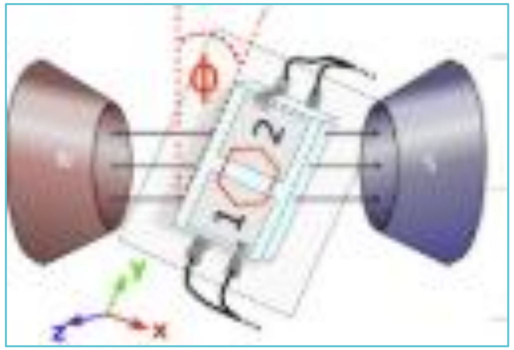

Thank you! Acknowledgments

- BMBF
- Bundesministerium für Bildung und Forschung

- Erforschung kondensierter Materie mit Großgeräten Ausbau und Unterhalt der Einrichtungen an ISOLDE/CERN

- Germany, contract: 05K16PGA and 05K22PGA for ISOSOL and for PACBIT Prof. Dr. D. Lupascu, Dr. J. H.-Schell

- European Union’s Horizon Europe Framework research and innovation programme
- Agreement no. 101057511 (EURO-LABS)

ISOLDE Solid State Physics

SPONSORED BY THE

Federal Ministry of Education and Research

EURO-LABS
EUROPEAN LABORATORIES FOR ACCELERATOR BASED SCIENCES

Prof. Lukas Eng
Spokesperson

Dr. Juliana Schell
Spokesperson

Mr. Thanh Dang
PhD candidate

Mr. Ian Yap
PhD Candidate

Mr. Hannes Gürlich
Master candidate

More researchers from TU-Dresden:
S. D. Seddon, B. Koppitz
Consultants:

A. M. L. Lopes, A. W. Carbonari,
B. P. Rocha-Rodrigues

home.cern

Mr. Björn Dörschel
Master candidate

Ms. Nicole Lima
PhD Candidate